Synthesis and Characterization of Hexagonal Boron Nitride Film as a Dielectric Layer for Graphene Devices

Ki Kang Kim,[†,‡] Allen Hsu,[†] Xiaoting Jia,[§] Soo Min Kim,[†] Yumeng Shi,[†] Mildred Dresselhaus,[†,⊥] Tomas Palacios,[†] and Jing Kong[†,*]

[†]Department of Electrical Engineering and Computer Sciences, Massachusetts Institute of Technology, Cambridge, Massachusetts 02139, United States, [‡]Nano Information Technology Academy (NITA), Dongguk University, Seoul 100-715, Republic of Korea, and [§]Department of Materials Science and Engineering and [⊥]Department of Physics, Massachusetts Institute of Technology, Cambridge, Massachusetts 02139, United States

ABSTRACT

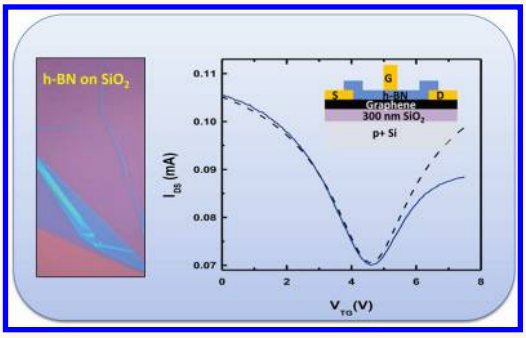

Hexagonal boron nitride (h-BN) is a promising material as a dielectric layer or substrate for two-dimensional electronic devices. In this work, we report the synthesis of large-area h-BN film using atmospheric pressure chemical vapor deposition on a copper foil, followed by Cu etching and transfer to a target substrate. The growth rate of h-BN film at a constant temperature is strongly affected by the concentration of borazine as a precursor and the ambient gas condition such as the ratio of hydrogen and nitrogen. h-BN films with different thicknesses can be achieved by controlling the growth time or tuning the growth conditions. Transmission electron microscope characterization reveals that these h-BN films are polycrystalline, and the *c*-axis of the crystallites points to different directions. The stoichiometry ratio of boron and nitrogen is close to 1:1, obtained by electron energy loss spectroscopy. The dielectric constant of h-BN film obtained by parallel capacitance measurements (25 μm^2 large areas) is 2–4. These CVD-grown h-BN films were integrated as a dielectric layer in top-gated CVD graphene devices, and the mobility of the CVD graphene device (in the few thousands $cm^2/(V \cdot s)$ range) remains the same before and after device integration.

KEYWORDS: hexagonal boron nitride · chemical vapor deposition · borazine · copper foil

Hexagonal boron nitride (h-BN) has recently attracted a lot of attention because of its similarity to graphene in structure and its very interesting suggested or demonstrated properties, such as UV emission,[1,2] exceptional mechanical and thermal properties, and chemical stability.[3−6] It has a layered structure like graphene/graphite, and within each layer, sp^2-bonded alternating boron and nitrogen atoms are arranged in a honeycomb lattice. Monolayer h-BN is another two-dimensional atomic layered material (just as graphene), and fascinating phenomena, such as a giant flexoelectric effect, have been predicted.[7] More importantly, h-BN has been shown to be a superior substrate for graphene devices, and with the same graphene material (either obtained by graphite exfoliation or synthesized by chemical vapor deposition (CVD)), the mobility values measured on an h-BN substrate are 1 order of magnitude higher than the mobility of the devices fabricated on SiO_2/Si substrate.[8,9] Therefore, high-quality h-BN material is critical for high-performance graphene devices, and it is highly desirable to develop effective synthesis methods.

Inspired by the graphene synthesis *via* CVD on metallic substrates, such as Co,[10] Pt,[11,12] Ir,[13] Ru,[14] Ni,[15−18] and Cu,[19,20] and by a viable transfer technique,[17,18,21−23] recently h-BN synthesis *via* CVD on Ni or Cu substrates was also further investigated.[9,24−26] Using either ammonia borane (H_3B-NH_3) or borazine ($B_3N_3H_6$), multilayer or monolayer h-BN could be synthesized by CVD and transferred to the desired substrates. In this work, h-BN films with thickness between 2 and ~20 nm were synthesized on Cu foil using borazine ($B_3N_3H_6$) as a precursor under atmospheric CVD (APCVD) and were integrated into graphene devices as the gate dielectric layer. We show in the present work that the thickness of the h-BN films can be controlled by the growth time or synthesis conditions. The CVD synthesis and transfer technique allows a straightforward integration of the h-BN films into graphene devices, and the devices show comparable performance before and after the h-BN integration.

* Address correspondence to jingkong@mit.edu.

Received for review April 16, 2012 and accepted September 12, 2012.

Published online September 12, 2012
10.1021/nn301675f

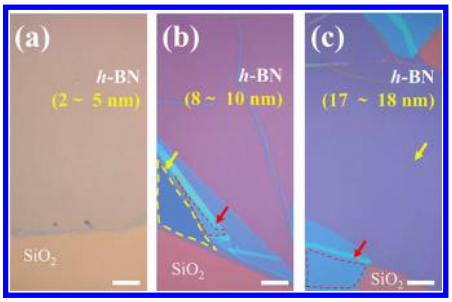

Figure 1. Optical images of h-BN films with different thicknesses on a SiO_2/Si substrate (the SiO_2 layer is 300 nm). The thickness of these films was measured by atomic force microscopy: (a) 2−5 nm, (b) 8−10 nm, and (c) 17−18 nm. The two yellow and two red arrows point out regions of similar thicknesses. The scale bar indicates 10 μm.

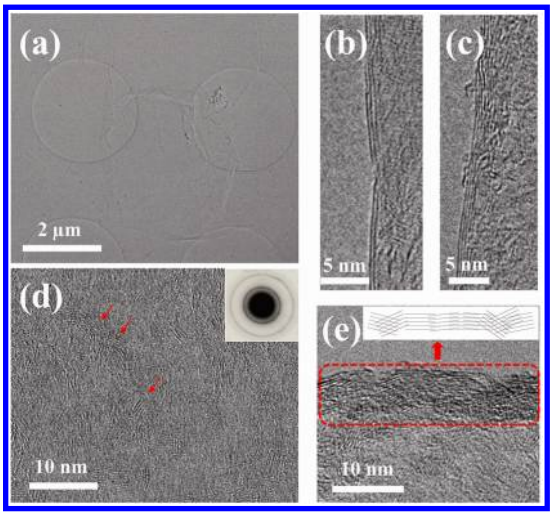

Figure 2. TEM images of the h-BN films. (a) Lower magnification image of a thin h-BN film (2−3 nm thick). TEM images of (b) 2−3 layer h-BN sample and (c) 4−5 layer h-BN sample at their folded edge. (d,e) TEM images of a thicker h-BN sample (>10 nm thick). In (d), the red arrow indicates regions showing fringes in the lattice. Inset in (d) shows the selective area diffraction pattern of this sample (2 μm sized area), indicating that the h-BN film is polycrystalline in structure. (e) TEM image of the folded edge of this sample, indicating that the *c*-axes of the crystallites are pointing in different directions, as illustrated by the inset in (e).

RESULTS AND DISCUSSION

The synthesis of h-BN film was carried out at 750 °C under a hydrogen and/or nitrogen atmosphere using Cu foil with atmospheric pressure CVD (APCVD), and then the h-BN on Cu was postannealed at 1000 °C for 1 h to improve the film crystallinity.[27] Since the precursor of borazine is a liquid under ambient conditions, a bubbler is used, and nitrogen is used as a carrier gas for the borazine. The growth rate of h-BN was controlled by the borazine bubbling rate and the ambient conditions of hydrogen and nitrogen. After the growth of h-BN, the film was transferred onto 300 nm SiO_2/Si using PMMA as a protection layer, as described elsewhere.[18]

Optical Contrast of the h-BN Films on 300 nm SiO_2/Si. Figure 1 shows the optical images of h-BN films with different thicknesses. The optical contrast is changed by the thickness of the films. It is noted that the film thickness is measured by atomic force microscopy (AFM) after the films are transferred onto a 300 nm SiO_2/Si substrate. When the thickness of the h-BN film is 2−5 nm, the color of the film barely shows a difference with that of the pristine substrate. However, as the thickness of the h-BN film increases, it is easier to distinguish between the substrate and the h-BN film, as shown in Figure 1b,c. As suggested by previous work,[28] the thickness could be estimated by comparing the optical contrast. For example, the optical contrast of the yellow dotted region (indicated by the yellow arrow) in Figure 1b, which is the 8−10 nm film being folded once, shows similar optical contrast as the film in Figure 1c, indicating that its thickness is around 16 nm. In addition, the thickness of the region outlined by the red dotted line in Figure 1b,c could be estimated to be ~36 nm with 4-fold folding in Figure 1b and 2-fold folding of the 17−18 nm film in Figure 1c. These results indicate that the thickness of the large-area h-BN grown by copper foil is quite uniform and can be controlled by synthesis conditions.

Structure Characterization of the h-BN Films by TEM. The structure of the h-BN films was characterized by transmission electron microscopy (TEM). Figure 2 shows the representative TEM images of various thicknesses of h-BN film. Most of the h-BN films are continuous over the TEM grid (Figure 2a). Figure 2b,c shows that the number of layers (as counted by the number of lines at the folding edge) in these samples were 2−3 and 4−7, respectively. At higher magnification in Figure 2d, fringe-like features (indicated by the red arrows) can be seen, which could be either due to lattice fringes or wrinkles in the h-BN layers or due to the fact that the *c*-axis orientation of the multilayer stacking is in the in-plane direction. If these features are due to the lattice fringes, as they are in different orientations, this suggests that we have a polycrystalline sample here, and the crystallites are ~10 nm. Indeed, the selected area electron diffraction (SAED) of a 2 μm area region in the inset of Figure 2d shows circular rings instead of individual spots, suggesting that the h-BN film has a polycrystalline structure for this 2 μm sized area. The edge of the sample in panel d is shown in Figure 2e, which also indicates that the crystallites of the multilayer h-BN stacks are randomly oriented, in contrast to the parallel straight lines observed in high-quality samples.[23] The schematic illustration in the inset of Figure 2e describes the polycrystalline structure of the h-BN film. The origin of the polycrystalline structure will be discussed in the later sections.

Elemental and Bonding Nature of the h-BN Films. To study the stoichiometry and atomic bonding nature of the boron and nitrogen atoms in the h-BN films, electron energy loss spectroscopy (EELS) was used. The elemental analysis of the h-BN film with the GIF (energy filtered imaging) technique was carried out during

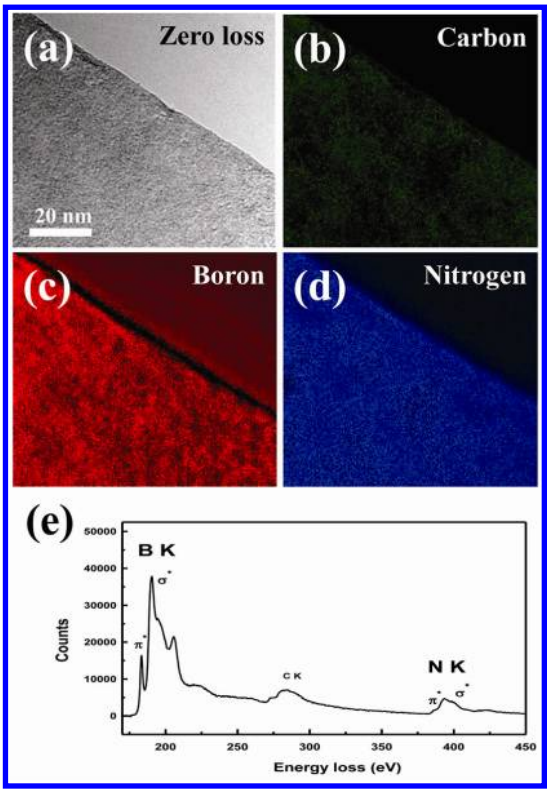

Figure 3. Elemental analysis of h-BN film by EELS. (a) Zero-loss TEM image of a h-BN film, GIF (energy-filtered imaging technique) imaging of (b) carbon, (c) boron, and (d) nitrogen. (e) Representative EELS spectra of h-BN film.

mapping. Compared to the zero-loss TEM image of the h-BN film (Figure 3a), Figure 3b–d shows the GIF imaging of carbon, boron, and nitrogen, respectively. First, boron and nitrogen are distributed uniformly throughout the sample, consistent with the fact that the sample is a boron–nitrogen compound. Carbon in the h-BN film is randomly distributed over the area. This is most likely due to the PMMA residuals which are left on the sample after the h-BN transfer process. The representative EELS spectrum in Figure 3e clearly shows the presence of the characteristic boron and nitrogen K-shell peaks. There is a weak carbon K-shell peak (near 280 eV) due to the residual PMMA.[29] A similar carbon peak in the EELS spectra was observed in the high-quality monolayer h-BN sample reported previously.[25] Also, the characteristic π^* and σ^* energy loss peaks at the boron and nitrogen K-shell are clearly shown, indicating the h-BN film has sp^2 hybridization bonds.[30] In addition, a close to 1:1 stoichiometry of the boron and nitrogen is obtained after integration of each characteristic peak.

Dielectric Constant Evaluation of the h-BN Films and Their Integration into Graphene Devices. The main effort in this work is to use the h-BN films as a dielectric layer for a graphene field effect transistor (FET). In order to evaluate the dielectric quality of our h-BN films, we fabricated metal–h-BN–metal capacitor structures to evaluate the dielectric constant (ε_r) and breakdown voltage (V_b) of these materials. The bottom Ti/Pt (2 nm/20 nm) "M1" electrodes in the inset in Figure 4a were patterned using standard photolithography and lift-off process. Large-area h-BN films (typically 15–19 nm thick) were then transferred onto the substrates having the electrodes. Finally, top electrodes (5 nm Ti/90 nm Au) "M2" were patterned using photolithography and lift-off. Capacitance was measured from 50 to 450 kHz using an Agilent 4294A impedance analyzer. The typical device size measured was 5 μm × 5 μm. The extracted average dielectric constant (ε) was 2–4 with a breakdown electric field of 1.5–2.5 MV/cm, as shown in Figure 4b. The lower breakdown field (~8 MV/cm for single-crystalline h-BN)[31] is most likely due to the polycrystalline nature of the h-BN films providing a leakage pathway through grain boundaries.

In addition, we fabricated top-gated graphene FET with transferred h-BN as a top-gate dielectric on top of CVD-grown graphene (inset of Figure 4c). To study the impact of h-BN on the transport of graphene, we fabricated van der Pauw structures to measure the Hall mobility before and after transfer of the h-BN. Using a magnetic field of B = 0.30 T, I = 1 mA, and an area of graphene of 100 μm × 100 μm, we measured a room temperature Hall hole mobility of 2455 $cm^2/(V\cdot s)$, a carrier density $n_s = 3.60 \times 10^{12}\ cm^{-2}$ before integrating the h-BN, and of 2141 $cm^2/(V\cdot s)$, $n_s = 4.81 \times 10^{12}\ cm^{-2}$ for the same device after transfer. Five other devices also showed similar Hall hole mobility values before and after the integration of h-BN. The increase in charge doping is most likely due to the wet transfer process that might trap water at the h-BN/CVD graphene interface. Figure 4c shows the measured drain-to-source (I_{DS}) *versus* normalized electrostatically gated carrier concentration ($n_G - n_{Dirac}$) of one of the transistors before and after h-BN integration measured first using the back gate and then finally measured using the top gate. The data are plotted in units of normalized electrostatically gated carrier concentration to allow top-gate and bottom-gate data to be plotted on the same axes. The fabrication technology for the graphene transistors is similar to the one used in our metal–h-BN–metal capacitors, except that the bottom electrode in Figure 4c is replaced with graphene. To extract the carrier mobility from the transfer curves, we used a simplified model to fit the device data including the effects of parasitic resistances.[32]

$$R_{tot} = \frac{V_{DS}}{I_{DS}} = 2\frac{R_c}{W} + \frac{L_G}{W}R_G$$

$$R_G = \frac{1}{q\mu_{Hall}n_{total}}$$

$$n_{total} = \sqrt{{n_i}^2 + \left(\frac{C_{ox}}{q}[V_G - V_{Dirac}]\right)^2}$$

$$n_G = \frac{C_{ox}}{q}V_G$$

$$n_{Dirac} = \frac{C_{ox}}{q}V_{Dirac}$$

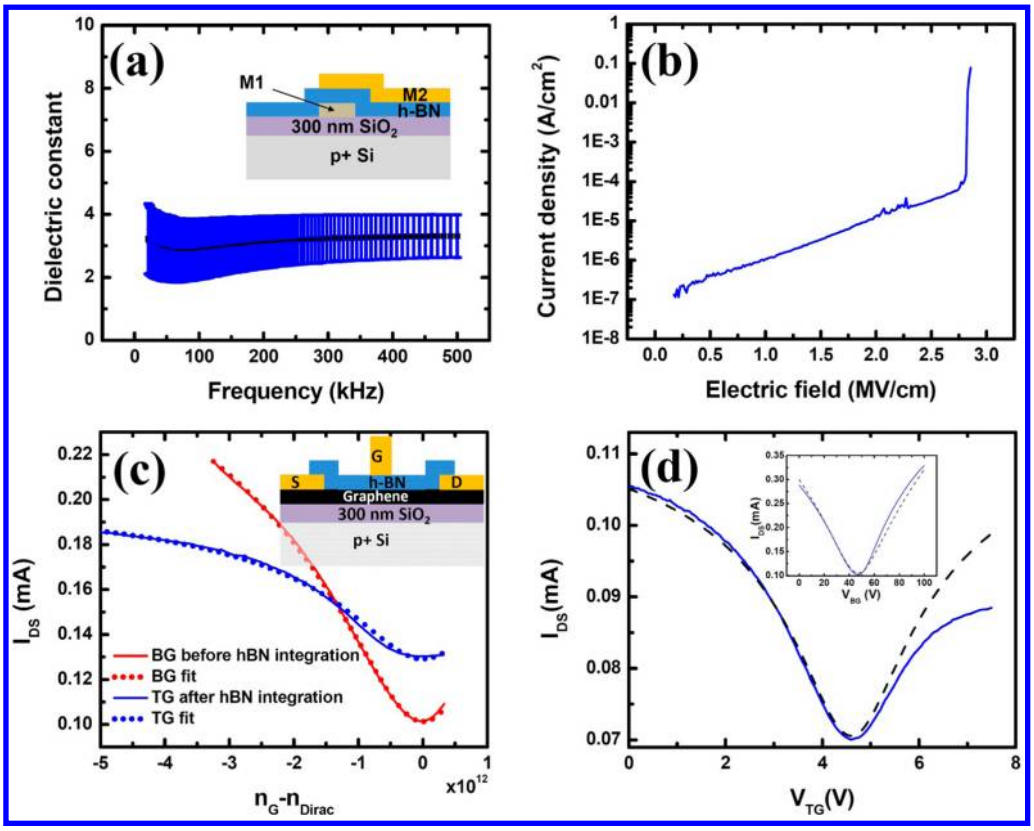

Figure 4. h-BN dielectric constant and graphene devices. (a) Average dielectric constant of h-BN film depending on frequency. (b) Representative breakdown voltage measurement. (c) Drain to source current (I_{DS}) *versus* normalized electrostatically gated carrier concentration ($n_G - n_{dirac}$) of a bottom-gated (BG) and top-gated (TG) graphene device before and after h-BN integration. The solid and dotted lines indicate the experimental data and fitted data, respectively. The schematic diagram of the graphene device is shown in the top inset. (d) $I_{DS}-V_{TG}$ characterization of another device after hBN integration, with a back-gate bias of −25 V, so that both p- and n-sides are observed in the measurement range. The characterization with the bottom gate before h-BN integration is shown in the inset. Dotted lines are fitted curve using the same model. V_{DS} for all measurements is 1 V.

where R_c is the contact resistance including the access resistance (*i.e.*, the resistance of the region not covered by top-gate metal), R_G is the channel graphene resistance, L_G is the gate length, W is width of the device, μ_{Hall} is the hall mobility, n_i is the residual charge impurity concentration, n_{total} is the total channel charge, C_{ox} is the gate dielectric capacitance, V_G is the applied gate voltage either on the top or back gate, and V_{Dirac} is the minimum conductivity point. Here the gate dielectric capacitance for the bottom gate (C_{BG}) can be calculated based on the SiO_2 thickness (11.5 nF/cm^2) and for the top gate, C_{TG} is obtained by comparing by the ratio of the Dirac voltage between bottom and top-gate measurements (115−184 nF/cm^2), which agrees well with our estimated dielectric constant as measured before.

In this study, back-gated measurements before h-BN integration are first fitted using the simplified model, which provides reasonable fits for contact resistances that agree well with transmission line measurements (TLM) (2−8 kΩ·μm). CVD-hBN is then integrated as a top-gate dielectric and then remeasured. The transfer curves are then fitted using the same model used previously. The reduced on-state current and transconductance in the top-gated devices is mostly attributed to increased contact resistances due to the ungated graphene regions. This can be easily explained due to the device geometry of our transistor. During back-gate measurements, the entire channel is modulated ($L = 6\ \mu$m, $W = 5\ \mu$m), while during top-gate measurements, only a fraction ($L = 3\ \mu$m) of our channel is modulated. The more pronounced sublinear dependence of I_D with respect to V_G in the top-gated case is encompassed within the model as a contact resistance term including any parasitic resistance such as access resistances and any additional resistances due to any Schottky or p−n junctions. The model and related fitting parameters are presented in Table 1. The field effect transistors also show a slightly increased p-type doping, agreeing well with Hall measurements. The discrepancy between the Hall hole mobility and the field effect hole mobility is due to the sample and transfer variations as different samples were used for Hall measurements and field effect mobility measurements.

All of our devices turn out to be heavily p-doped after h-BN integration. Figure 4d shows $I_{DS}-V_{TG}$ measurement from another device, where a back-gate bias (−25 V) was applied to ensure that both p- and n-side

TABLE 1. Fitting Parameters for the Top- and Back-Gated h-BN/Graphene Devices Shown in Figure 4c

parameter	unit	back gate (BG) before hBN integration	top gate (TG) after hBN integration
R_c	Ω-μm	7338	12130
μ_{Hall}	$cm^2/(V \cdot s)$	1338	1404
n_i	$1/cm^2$	8.078×10^{11}	9.228×10^{11}
n_{Dirac}	$1/cm^2$	3.25×10^{12}	5.9×10^{12}
C_{BG}	nF/cm^2	11.5	
C_{TG}/C_{BG}			11.5
W	μm	5	5
L_G	μm	6	3
L_{DS}	μm	6	6

conduction can be observed in the measurement range. The $I_{DS}-V_{BG}$ curve before the h-BN integration is shown in the inset of Figure 4d as a comparison. The same model was used to fit the measurement data, and similar mobility values before and after h-BN integration were again obtained. The curve fittings are shown as a dotted line in Figure 4d. The deviation in the fitting on the n-side is due to change in contact resistance caused by p−n junctions as well as possible deviation between electron and hole mobility.

Understanding the Synthesis of h-BN films *via* APCVD on Cu Foils. *1. Growth Rate of h-BN Films.* In order to control the h-BN film thickness, systematic studies were carried out in terms of growth rate. Figure 5a shows the h-BN film thickness (measured by AFM after transferring the film on 300 nm SiO_2/Si) as a function of growth time for 1 sccm borazine bubbling rate and 2000 sccm H_2 flow rate at a growth temperature of 750 °C. The film thickness shows a linear dependence on growth time, indicating the growth rate, which is defined by the film thickness per growth time, is constant and the film thickness can be controlled by the growth time. Figure 5b,c shows the effect of growth conditions on the growth rate. First, the effect of the borazine concentration was examined. With increasing borazine bubbling rate under 1000 sccm N_2, the growth rate is increased, but the increase in growth rate is not a linear behavior, as shown in Figure 5b. This is likely due to the fact that excess borazine does not participate in the growth of the h-BN film. From Figure 5, it is therefore concluded that 1−1.5 sccm of borazine is a suitable flow rate for growth. On the other hand, the growth rate at a constant of borazine bubbling rate is linearly increased by the amount of N_2 relative to H_2, as shown in Figure 5c. This effect can be understood by Le Chatelier's principle with the reaction below:

$$B_3N_3H_6 \leftrightarrow 3BN + 3H_2$$

If the partial pressure of hydrogen is increased, the equilibrium is shifted to counteract the imposed change, leading to a decreased growth rate. As a result, the growth rate in only a nitrogen atmosphere is about 2.3 times higher than that in a hydrogen atmosphere.

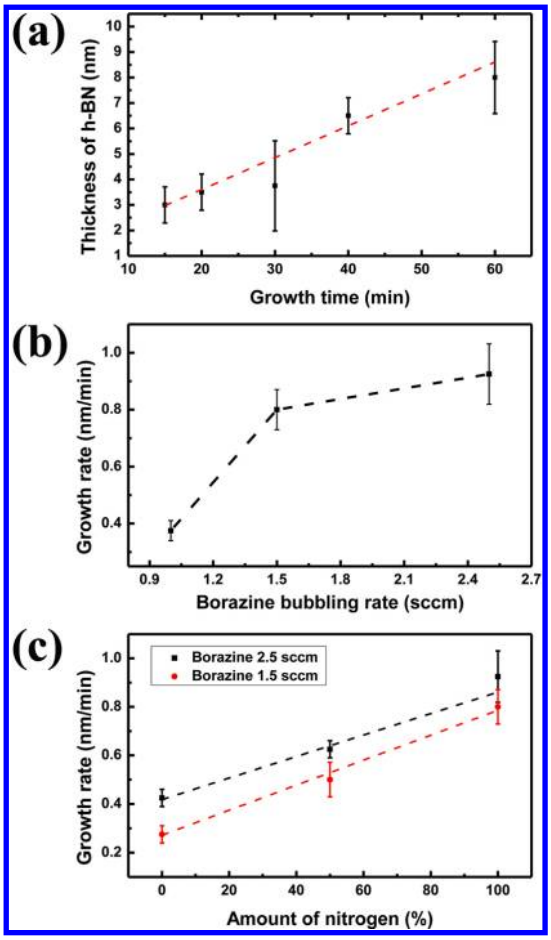

Figure 5. Control of the h-BN thickness. (a) Thickness of the h-BN film as a function of the growth time. Synthesis condition: borazine bubbling rate is 1 sccm, with 2000 sccm H_2, growth at 750 °C. Growth rate of the h-BN film (b) as a function of borazine bubbling rate under 1000 sccm N_2 atmophere and (c) as a function of the amount of N_2 relative to H_2. Total flow rate of nitrogen and hydrogen is 1000 sccm.

2. Growth Mechanism of h-BN Film on Copper Foil with Borazine. From the structural analysis described above, it was found that the resultant h-BN films are polycrystalline with crystallite sizes of ~10 nm. The film quality is not as high as the h-BN films grown with Ni thin film,[24] where much larger (~1 μm) single-crystalline domains were obtained. However, it was found that the h-BN films grown on the Ni thin film substrate were leaky as a dielectric layer, possibly due to the nonuniform regions grown at the Ni grain boundaries. For the Ni thin film substrate, after annealing at high temperature, deep grooves develop between the Ni grains. In contrast, the grain boundary grooves in the Cu foil are much shallower. Furthermore, the typical grain size of the Cu foil is >1 × 1 mm^2, much larger than that of the Ni grains (~20 × 20 μm^2). Therefore, Cu foil was used to achieve leakage-free h-BN films in this work.

The growth of the h-BN synthesis was carried out under atmospheric pressure CVD (APCVD) at various temperatures. According to the previous analysis,[27,33] the growth of h-BN film occurs *via* a thermal polymerization

process and could be divided to three steps: (I) adsorption of borazine or polyborazylene on the surface (−133 to 400 °C);[24,34] (II) thermally induced polymerization to form polyborazylene and the crossing linking reaction of B−H and N−H groups on adjacent chains (70−600 °C);[27,34,35] (III) dehydrogenation of the polyborazylene thin film to become a h-BN film (>700 °C).[24] Step I depends on the binding energy between the borazine molecule and the substrate.[34,36] Steps I and II play a crucial role in the formation of the h-BN film on the substrate. The temperature range of these steps is fairly wide in our experiments. We studied the growth from 300 to 1000 °C. The growth rate and the results are very different depending on the growth temperature. Generally, it was observed that, with higher growth temperature and borazine concentration, a higher growth rate is obtained. At higher temperature (>900 °C), the thickness is not easy to control due to the too high growth rate in our current setup (the lower limit of the flow rate for the borazine carrier gas is 0.5 sccm). Under high growth rate, a very rough surface was observed, with a large quantity of particles on the surface. This is because the thermally activated polymerization and dehydrogenation at higher temperature occur at the same time. It should be noted that since our current APCVD setup is a hot-wall reactor, the borazine at high temperature can be thermally activated before arriving at the substrate. We expect that the moderate growth temperature (750 °C) in this work could induce the fast polymerization and slight dehydrogenation of borazine, leading to the formation of polycrystalline h-BN film (Figure 2). In an ultrahigh vacuum (UHV) system, monolayer h-BN can be grown on various catalytic substrates such as Ni, Cu, Pt, Rh, and Rd at temperatures higher than 750 °C as reported previously[37−39] because the amount of borazine precursor introduced is only about few Langmuir, leading to surface-limited growth. Therefore, in order to improve the quality of the h-BN material in the future, a lower borazine concentration should be used or low-pressure CVD (LPCVD) systems should be considered. A cold-wall reactor could be another option to prevent thermal decomposition before the precursors reach the growth substrate.

CONCLUSION

In this work, we present the synthesis of large-area h-BN on copper foil and the integration of such films as a gate dielectric in graphene devices. The thickness of the h-BN films can be controlled by different growth conditions and growth times. The h-BN films are polycrystalline with crystallite sizes of ∼10 nm. The graphene-based transistors with h-BN gate dielectrics showed comparable performance before and after the h-BN integration. Future investigation to use the h-BN as both a bottom substrate and top gate for graphene devices will be developed, and further understanding of the growth mechanism will guide future improvements of the synthesis process and the quality of the h-BN thin films. This result will be applicable to both graphene devices and flexible electronics in the future.

EXPERIMENTAL SECTION

h-BN Growth Procedure. Borazine is used as a precursor for the h-BN synthesis in this work. Since borazine is a liquid, during the synthesis, it is delivered to the growth chamber by nitrogen carrier gas through a bubbler. The temperature of borazine is maintained at 0 °C using a commercial wine cooler. Before the h-BN growth, a copper foil (25 μm, 99.8%, Alfa Asear) which is used as a catalytic substrate is annealed at 1000 °C for 30 min under 10 sccm hydrogen atmosphere (LPCVD process), in order to increase the copper grain size and to obtain a smooth surface. The growth of h-BN is carried out at 750 °C for typically 5−30 min under 1−3 sccm of borazine under 2000 sccm of hydrogen. To study the effect of the ambient condition, the ratio of hydrogen and nitrogen flow rate (sccm) is varied between 0:1000 and 1000:0. After growth, the h-BN film on copper is post-annealed at 1000 °C for 1 h under 100 sccm hydrogen and 100 sccm nitrogen atmosphere.

Graphene Growth Procedure. Graphene was synthesized by LPCVD using a copper foil (25 μm, 99.8% Alfa Asear) as a catalytic metal substrate. Before graphene growth, the copper foil was annealed at 1000 °C for 30 min under 10 sccm hydrogen atmosphere (∼330 mTorr) to increase the grain size and to ensure the growth of a smooth surface, followed by synthesizing graphene under 15 and 50 sccm of methane and hydrogen atmospheres, respectively, for 40 min (∼1.5 Torr), while maintaining the same temperature. During the cooling step, 10 sccm of hydrogen was flowed until room temperature was reached.

Transfer. Poly(methyl methacrylate) (PMMA) (4.5% in anisole) was spun on the h-BN or graphene on copper foil at 2500 rpm for 1 min, followed by etching copper with copper etchant (CE-100, Transene). The film of PMMA/h-BN was washed by DI water to remove the residual copper etchant. To remove the residual iron particles which came from the copper etchant ($FeCl_3$), the film was floated on 10% HCl for 20 min, followed by neutralizing with deionized water. After the PMMA/h-BN film was transferred onto either SiO_2/Si or a quantifoil TEM grid (2.5 μm hole, Tel Pella), PMMA was removed by acetone vapor and thermal annealing at 450 °C for 2 h under an H_2/Ar atmosphere.

Device Fabrication. Metal−BN−metal capacitors were fabricated using standard photolithography techniques using an image reversal resist (AZ5214E from Microchem). Hybrid graphene/BN structures were fabricated following similar procedures. CVD graphene grown from copper was transferred onto thermally grown silicon dioxide on doped silicon. Ti/Pd/Au (25/450/150 Å) ohmic metal contacts were patterned using a lift-off process, and then the h-BN film was transferred on top. The graphene/BN stack was then patterned using a reactive oxygen etch with a photoresist hardmask. The top-gate metal contact was patterned from Ti/Au (500/2300 Å) again using an image reversal resist and lift-off.

Characterization. A TEM (JEOL 2010) instrument equipped with electron energy loss spectroscopy (EELS) and selected area electron diffraction (SAED) was used to characterize the structure of h-BN. The surface morphology of the copper foil and h-BN was examined by atomic force microscopy (Dimension 3100, Veeco). Optical absorption spectra of the samples were obtained by using a Varian Cary 500i instrument. The capacitance was measured using an Agilent 4294A impedance analyzer from 50 to 450 kHz. Electrical and Hall measurements were

done using an Agilent semiconductor parameter analyzer 4155C and a Hall effect probe station using a permanent neodymium magnet. Current–voltage sweeps were done in a Lakeshore Cryogenic Probe Station at room temperature.

Conflict of Interest: The authors declare no competing financial interest.

Acknowledgment. This work is partially supported by the National Science Foundation under award number NSF DMR 0845358 and the Materials, Structures and Device (MSD) Center, one of the five programs in the focus center research program (FCRP), a Semiconductor Research Corporation program. A.H. acknowledges the support from the MIT/Army Institute for Soldier Nanotechnologies (ISN) and the Army Research Laboratory. J.K., X.J., and M.D. acknowledge the Graphene Approaches to Terahertz Electronics (GATE) - MURI grant N00014-09-1-1063.

REFERENCES AND NOTES

1. Watanabe, K.; Taniguchi, T.; Kanda, H. Direct-Bandgap Properties and Evidence for Ultraviolet Lasing of Hexagonal Boron Nitride Single Crystal. *Nat. Mater.* **2004**, *3*, 404–409.
2. Kubota, Y.; Watanabe, K.; Tsuda, O.; Taniguchi, T. Deep Ultraviolet Light-Emitting Hexagonal Boron Nitride Synthesized at Atmospheric Pressure. *Science* **2007**, *317*, 932–934.
3. Lipp, A.; Schwetz, K. A.; Hunold, K. Hexagonal Boron Nitride: Fabrication, Properties and Applications. *J. Eur. Ceram. Soc.* **1989**, *5*, 3–9.
4. Kho, J. G.; Moon, K. T.; Kim, J. H.; Kim, D. P. Properties of Boron Nitride (BxNy) Films Produced by the Spin-Coating Process of Polyborazine. *J. Am. Ceram. Soc.* **2000**, *83*, 2681–2683.
5. Chen, Y.; Zou, J.; Campbell, S. J.; Le Caer, G. Boron Nitride Nanotubes: Pronounced Resistance to Oxidation. *Appl. Phys. Lett.* **2004**, *84*, 2430–2432.
6. Paine, R. T.; Narula, C. K. Synthetic Routes to Boron-Nitride. *Chem. Rev.* **1990**, *90*, 73–91.
7. Naumov, I.; Bratkovsky, A. M.; Ranjan, V. Unusual Flexoelectric Effect in Two-Dimensional Noncentrosymmetric sp^2-Bonded Crystals. *Phys. Rev. Lett.* **2009**, *102*, 217601/1-4.
8. Dean, C. R.; Young, A. F.; Meric, I.; Lee, C.; Wang, L.; Sorgenfrei, S.; Watanabe, K.; Taniguchi, T.; Kim, P.; Shepard, K. L.; *et al.* Boron Nitride Substrates for High-Quality Graphene Electronics. *Nat. Nanotechnol.* **2010**, *5*, 722–726.
9. Lee, K. H.; Shin, H.-J.; Lee, J.; Lee, I.-Y.; Kim, G.-H.; Choi, J.-Y.; Kim, S.-W. Large-Scale Synthesis of High-Quality Hexagonal Boron Nitride Nanosheets for Large-Area Graphene Electronics. *Nano Lett.* **2012**, *12*, 714–718.
10. Vaari, J.; Lahtinen, J.; Hautojarvi, P. The Adsorption and Decomposition of Acetylene on Clean and K-Covered Co(0001). *Catal. Lett.* **1997**, *44*, 43–49.
11. Ueta, H.; Saida, M.; Nakai, C.; Yamada, Y.; Sasaki, M.; Yamamoto, S. Highly Oriented Monolayer Graphite Formation on Pt(111) by a Supersonic Methane Beam. *Surf. Sci.* **2004**, *560*, 183–190.
12. Starr, D. E.; Pazhetnov, E. M.; Stadnichenko, A. I.; Boronin, A. I.; Shaikhutdinov, S. K. Carbon Films Grown on Pt(111) as Supports for Model Gold Catalysts. *Surf. Sci.* **2006**, *600*, 2688–2695.
13. Gall, N. R.; Rut'kov, E. V.; Tontegode, A. Y. Interaction of Silver Atoms with Iridium and with a Two-Dimensional Graphite Film on Iridium: Adsorption, Desorption, and Dissolution. *Phys. Solid State* **2004**, *46*, 371–377.
14. Sutter, P. W.; Flege, J.-I.; Sutter, E. A. Epitaxial Graphene on Ruthenium. *Nat. Mater.* **2008**, *7*, 406–411.
15. Shelton, J. C.; Patil, H. R.; Blakely, J. M. Equilibrium Segregation of Carbon to a Nickel (111) Surface–Surface Phase-Transition. *Surf. Sci.* **1974**, *43*, 493–520.
16. Eizenberg, M.; Blakely, J. M. Carbon Monolayer Phase Condensation on Ni(111). *Surf. Sci.* **1979**, *82*, 228–236.
17. Kim, K. S.; Zhao, Y.; Jang, H.; Lee, S. Y.; Kim, J. M.; Kim, K. S.; Ahn, J.-H.; Kim, P.; Choi, J.-Y.; Hong, B. H. Large-Scale Pattern Growth of Graphene Films for Stretchable Transparent Electrodes. *Nature* **2009**, *457*, 706–710.
18. Reina, A.; Jia, X.; Ho, J.; Nezich, D.; Son, H.; Bulovic, V.; Dresselhaus, M. S.; Kong, J. Few-Layer Graphene Films on Arbitrary Substrates by Chemical Vapor Deposition. *Nano Lett.* **2009**, *9*, 30–35.
19. Li, X.; Cai, W.; An, J.; Kim, S.; Nah, J.; Yang, D.; Piner, R.; Velamakanni, A.; Jung, I.; Tutuc, E.; *et al.* Large-Area Synthesis of High-Quality and Uniform Graphene Films on Copper Foils. *Science* **2009**, *324*, 1312–1314.
20. Bhaviripudi, S.; Jia, X. T.; Dresselhaus, M. S.; Kong, J. Role of Kinetic Factors in Chemical Vapor Deposition Synthesis of Uniform Large Area Graphene Using Copper Catalyst. *Nano Lett.* **2010**, *10*, 4128–4133.
21. Bae, S.; Kim, H.; Lee, Y.; Xu, X.; Park, J.-S.; Zheng, Y.; Balakrishnan, J.; Lei, T.; Kim, H. R.; Song, Y. I.; *et al.* Roll-to-Roll Production of 30-Inch Graphene Films for Transparent Electrodes. *Nat. Nanotechnol.* **2010**, *5*, 574–578.
22. Han, G. H.; Shin, H.-J.; Kim, E. S.; Chae, S. J.; Choi, J.-Y.; Lee, Y. H. Poly(ethylene-*co*-vinyl acetate)-Assisted One-Step Transfer of Ultra-large Graphene. *Nano* **2011**, *6*, 59–65.
23. Kim, K. K.; Reina, A.; Shi, Y.; Park, H.; Li, L.-J.; Lee, Y. H.; Kong, J. Enhancing the Conductivity of Transparent Graphene Films *via* Doping. *Nanotechnology* **2010**, *21*, 285205/1-6.
24. Shi, Y.; Hamsen, C.; Jia, X.; Kim, K. K.; Reina, A.; Hofmann, M.; Hsu, A. L.; Zhang, K.; Li, H.; Juang, Z.-Y.; *et al.* Synthesis of Few-Layer Hexagonal Boron Nitride Thin Film by Chemical Vapor Deposition. *Nano Lett.* **2010**, *10*, 4134–4139.
25. Kim, K. K.; Hsu, A.; Jia, X.; Kim, S. M.; Shi, Y.; Hofmann, M.; Nezich, D.; Rodriguez-Nieva, J. F.; Dresselhaus, M.; Palacios, T.; *et al.* Synthesis of Monolayer Hexagonal Boron Nitride on Cu Foil Using Chemical Vapor Deposition. *Nano Lett.* **2012**, *12*, 161–166.
26. Song, L.; Ci, L.; Lu, H.; Sorokin, P. B.; Jin, C.; Ni, J.; Kvashnin, A. G.; Kvashnin, D. G.; Lou, J.; Yakobson, B. I.; *et al.* Large Scale Growth and Characterization of Atomic Hexagonal Boron Nitride Layers. *Nano Lett.* **2010**, *10*, 3209–3215.
27. Fazen, P. J.; Remsen, E. E.; Beck, J. S.; Carroll, P. J.; McGhie, A. R.; Sneddon, L. G. Synthesis, Properties, and Ceramic Conversion Reactions of Polyborazylene—A High Yoeld Polymeric Precursor to Boron-Nitride. *Chem. Mater.* **1995**, *7*, 1942–1956.
28. Gorbachev, R. V.; Riaz, I.; Nair, R. R.; Jalil, R.; Britnell, L.; Belle, B. D.; Hill, E. W.; Novoselov, K. S.; Watanabe, K.; Taniguchi, T.; *et al.* Hunting for Monolayer Boron Nitride: Optical and Raman Signatures. *Small* **2011**, *7*, 465–468.
29. Silva, S. R. P. *INSPEC, The Institution of Electrical Engineers*, London, Uinted Kindom, 2003.
30. Huang, J. Y.; Yasuda, H.; Mori, H. HRTEM and EELS Studies on the Amorphization of Hexagonal Boron Nitride Induced by Ball Milling. *J. Am. Ceram. Soc.* **2000**, *83*, 403–409.
31. Young, A. F.; Dean, C. R.; Meric, I.; Sorgenfrei, S.; Ren, H.; Watanabe, K.; Taniguchi, T.; Hone, J.; Shepard, K. L.; Kim, P. Measurement of the Electronic Compressibility of Bilayer Graphene. *Phys. Rev. B* **2010**, *82*, 041412/1-1.
32. Kim, S.; Nah, J.; Jo, I.; Shahrjerdi, D.; Colombo, L.; Yao, Z.; Tutuc, E.; Banerjee, S. K. Realization of a High Mobility Dual-Gated Graphene Field-Effect Transistor with Al_2O_3 Dielectric. *Appl. Phys. Lett.* **2009**, *94*, 062107/1-3.
33. Fazen, P. J.; Beck, J. S.; Lynch, A. T.; Remsen, E. E.; Sneddon, L. G. Thermally Induced Borazine Dehydropolymerization Reactions. Synthesis and Ceramic Conversion Reactions of a New High-Yield Polymeric Precursor to Boron-Nitride. *Chem. Mater.* **1990**, *2*, 96–97.
34. Paffett, M. T.; Simonson, R. J.; Papin, P.; Paine, R. T. Borazine Adsorption and Decomposition at Pt(111) and Ru(001) Surface. *Surf. Sci.* **1990**, *232*, 286–296.
35. Chan, V. Z. H.; Rothman, J. B.; Palladino, P.; Sneddon, L. G.; Composto, R. Characterization of Boron Nitride Thin Films Prepared from a Polymer Precursor. *J. Mater.Res.* **1996**, *11*, 373–380.
36. Laskowski, R.; Blaha, P.; Schwarz, K. Bonding of Hexagonal BN to Transition Metal Surfaces: An *Ab Initio* Density-Functional Theory Study. *Phys. Rev. B* **2008**, *78*, 045409/1-10.
37. Preobrajenski, A. B.; Vinogradov, A. S.; Martensson, N. Monolayer of h-BN Chemisorbed on Cu(111) and Ni(111): The Role

of the Transition Metal 3d States. *Surf. Sci.* **2005**, *582*, 21–30.
38. Preobrajenski, A. B.; Vinogradov, A. S.; Ng, M. L.; Cavar, E.; Westerstrom, R.; Mikkelsen, A.; Lundgren, E.; Martensson, N. Influence of Chemical Interaction at the Lattice-Mismatched h-BN/Rh(111) and h-BN/Pt(111) Interfaces on the Overlayer Morphology. *Phys. Rev. B* **2007**, *75*, 245412/1-8.
39. Morscher, M.; Corso, M.; Greber, T.; Osterwalder, J. Formation of Single Layer h-BN on Pd(111). *Surf. Sci.* **2006**, *600*, 3280–3284.